HHS Public Access

Author manuscript

Mol Cancer Res. Author manuscript; available in PMC 2024 September 01.

Published in final edited form as:

Mol Cancer Res. 2024 March 01; 22(3): 254–267. doi:10.1158/1541-7786.MCR-23-0955.

FGFR1 signaling facilitates obesity-driven pulmonary outgrowth in metastatic breast cancer

Eylem Kulkoyluoglu Cotul[1], **Muhammad Hassan Safdar**[1], **Sebastian Juan Paez**[1], **Aneesha Kulkarni**[1], **Mitchell G. Ayers**[1], **Hang Lin**[1], **Zilin Xianyu**[1], **Dorothy Teegarden**[2,3], **Stephen D. Hursting**[4,5,6], **Michael K. Wendt**[1,2,*]

[1]Department of Medicinal Chemistry and Molecular Pharmacology, Purdue University, West Lafayette, IN, United States.

[2]Purdue University Institute for Cancer Research, Purdue University, West Lafayette, IN, United States

[3]Department of Nutrition Science, Purdue University, West Lafayette, IN, United States.

[4]Lineberger Comprehensive Cancer Center, University of North Carolina at Chapel Hill, Chapel Hill, NC, United States.

[5]Nutrition Research Institute, University of North Carolina at Chapel Hill, Kannapolis, NC, United States.

[6]Department of Nutrition, University of North Carolina at Chapel Hill, Chapel Hill, NC, United States

Abstract

Survival of dormant, disseminated breast cancer (BC) cells contributes to tumor relapse and metastasis. Women with a body mass index greater than 35 have an increased risk of developing metastatic recurrence. Herein, we investigated the effect of diet-induced obesity (DIO) on primary tumor growth and metastatic progression using both metastatic and systemically dormant mouse models of BC. This approach led to increased PT growth and pulmonary metastasis. We developed a novel protocol to induce obesity in Balb/c mice by combining dietary and hormonal interventions with a thermoneutral housing strategy. In contrast to standard housing conditions, ovariectomized Balb/c mice fed a high fat diet under thermoneutral conditions became obese over a period of 10 weeks, resulting in a 250% gain in fat mass. Obese mice injected with the D2.OR model developed macroscopic pulmonary nodules compared to the dormant phenotype of these cells in mice fed a control diet. Analysis of the serum from obese Balb/c mice revealed increased levels of fibroblast growth factor 2 (FGF2) as compared to lean mice. We demonstrate that serum from obese animals, exogenous FGF stimulation, or constitutive stimulation through autocrine and paracrine FGF2 is sufficient to break dormancy and drive pulmonary outgrowth. Blockade of fibroblast growth factor receptor (FGFR) signaling or specific depletion of FGFR1 prevented obesity-associated outgrowth of the D2.OR model.

[*]**To whom correspondence should be addressed:** Michael K. Wendt, mwendt@purdue.edu, 201 S. University Street, West Lafayette, IN 47906. Phone: 765-494-0860.

Disclosure of Potential Conflicts of interest: The authors declare no conflicts of interest.

Introduction:

Breast cancer is the most common cancer type in women worldwide. Due to early diagnosis and surgical interventions developed in the last two decades, 5-year survival rates for localized disease are above 90% (1). In contrast, almost 10–20% of patients experience tumor recurrence and distant organ metastases beyond 5 years from the original diagnosis (2), and most of these patients are lost because of the recalcitrant nature of metastatic disease.

It is clear that tumor cells disseminate throughout the body very soon after formation of the primary tumor. Maintenance of a dormant state is a major underlying factor contributing to disease remission following removal of the primary tumors. Breakage of this dormancy leads to the development of recurrent metastatic lesions throughout the body. Thus, there is a critical need to understand the biology of dormancy to maintain this state and prevent disease progression. Preclinical studies support the notion that obesity is a major contributing factor to tumor recurrence, increasing the risk of distant-organ metastases occurring 5–10 years after treatment (3,4).

Fibroblast growth factor receptor (FGFR) signaling acts as a metabolic regulator. Recent studies indicate a genetic association between FGFR signaling and obesity-associated factors, such as leptin (5–7). FGFR activation under obese conditions correlates with shorter disease-free survival in breast cancer patients receiving ER-targeting therapies [8]. Together with FGFR, separate studies indicate that adipose tissue is a rich source for FGFR ligands, including FGF1 and FGF2 (9,10). In addition, FGF2 stimulates adipogenic differentiation in human adipose-derived stem cells (11,12). In certain ER+ breast cancer cells, FGF2 stimulation promotes the survival of breast cancer cells but inhibits metastasis through stabilization of a dormancy-associated epithelial-mesenchymal transition (EMT) (13),(14). In contrast, several clinical studies have revealed a strong correlation between high plasma FGF2 levels, obesity, and disease progression (15–17). Therefore, we still lack a complete understanding of how FGFR signaling influences obesity-associated breast cancer progression.

In this study, we utilized thermoneutral housing conditions in combination with ovariectomy to develop a novel *in vivo* system to study how diet-induced obesity (DIO) affects breast cancer metastasis. Through this process, we characterized the role of FGFR1 signaling under these clinically relevant conditions. In addition to metastatic models, we utilized the D2.OR model of pulmonary dormancy (18–20). These cells remain viable, but dormant when delivered to the lungs of lean mice fed standard chow (18). Use of bioluminescent imaging allowed us to quantify the presence of these dormant lesions and assess how DIO and FGF signaling perturb this asymptomatic state. Taken together, our data indicate that increased systemic levels of FGF2 contribute to breakage of pulmonary tumor dormancy and obesity-associated metastatic disease progression.

Material and Methods:

Cell culture and reagents

The murine breast cancer cell lines E0771 (CRL-3461) and NMuMG (CRL-1636) cells were purchased from the American Type Culture Collection (ATCC, Manassas, VA). 4T1 and D2.OR cell lines were a kind gift from Fred R. Miller (21). They were constructed to express non-immunogenic levels of firefly luciferase via stable transfection under zeocin selection (18,22,23). E0771, 4T1 and D2.OR cell lines were cultured with regular Dulbecco's Modified Eagle Medium (DMEM) (Cytiva, SH30022.01, Marlborough, MA) with 10% (v/v) FBS (Gibco, Grand Island, NY) and 1% (v/v) penicillin and streptomycin (Gibco PenStrep, 15140122, Grand Island, NY). NMuMG cells were cultured with regular DMEM with 10% (v/v) FBS, 1% (v/v) penicillin and streptomycin and 0.5% insulin (Millipore, I9278–5ML). All cell lines were cultured at 37°C with 5% CO_2 and they were tested for mycoplasma contamination regularly (every 6 months) by using qRT-PCR method with targeted primers. Cell lines were authenticated via IDEXX cell check 19 mouse plus.

Animal models

All *in vivo* experiments were conducted based on protocols approved by Purdue University and following the National Institutes of Health standards for use and care of animals (IACUC Protocol # 1310000978). Where indicated mice were ovariectomized and housed at ~80°F. Diet induced obesity was verified by gain in fat mass as determined by Echo MRI body composition analyzer. For tail vein inoculation experiments, firefly luciferase-expressing E0771 (1×10^6/100μl) cells were injected into the lateral tail vein of female 6-weeks-old C57BL6/J mice (Jackson Laboratories). Pulmonary tumor growth was tracked using an Advanced Molecular Imager (AMI) (Spectral Instruments, Tucson, AZ). For orthotopic mammary fat pad injections, E0771 cells (5×10^5/50μl) were transplanted into the fourth fat pad of C57BL6/J mice. Primary tumor growth was quantified using caliper measurement and pulmonary metastasis was monitored using the AMI imager. All experiments using D2.OR and 4T1 cells were initiated using ovariectomized, 6-week-old, female, Balb/c mice housed at thermoneutral temperatures. D2.OR cells were delivered via tail vein inoculation (1×10^6/100μl) and 4T1 cells were delivered via an intraductal injection into the mammary fat pad (5×10^4/50μl). In some instances D2.OR cells were administered via sequential injections, administered at the indicated time points. For this approach, the maintenance of a dormant phenotype in the control conditions was continuously monitored by bioluminescent imaging. Where indicated E0771 and 4T1 primary tumors were removed by surgical excision in a survival surgery and mice were monitored for metastasis.

For DIO studies, C57BL6/J mice were fed either a 60% (Research Diets # D12492) or 10% (D12450J) fat diet for the indicated amounts of time. Balb/c mice were fed the same diets, but mice were housed at thermal neutral temperatures (27–30°C). For all tumor engraftment studies, Balb/c mice were also ovariectomized prior to initiation of thermoneutral housing and a fat-controlled diet.

Immunoblot Analyses

Cells (3×10^5) were seeded and treated with different ligand and targeting agents. Protein isolation procedure was performed by using a modified radioimmunoprecipitation assay (RIPA) buffer including protease inhibitor (P8340, Sigma-Aldrich, St. Louis. MO)(23,24). Protein concentrations were determined using a BCA protein assay (23225, Novagen, Darmstadt, Germany). Protein isolates were mixed with 6x Laemmli sample buffer and boiled for 5 minutes. All samples were run on 10% polyacrylamide gels, and they underwent electrophoretic separation in 1x Tris-Glycine buffer. Proteins were transferred onto PVDF membrane (IPVH00010, Immobilon®,Darmstadt, Germany). Membranes were incubated at 4°C overnight with primary antibodies for FGFR1 (CST 9740S, 1:1000), FGF2 (abcam, ab208687, 1:1000) anti-phospho AKT (CST 9271S, 1:1000), anti-AKT (CST 9272S, 1:1000), anti-phospho-ERK (CST 9101S, 1:1000) and anti-ERK (CST 4696S, 1:1000) (Cell Signaling Inc., MA, USA) in 5% BSA in 1x TBS-T buffer. The next day, membranes were washed with 1x TBS-T buffer three times for 5 minutes and incubated with goat anti-Rabbit-HRP (65–6120, 1:2000) or goat anti-Mouse-HRP (62–6520,1:2000) secondary antibodies for 1 hour at room temperature (Invitrogen; Camarillo, CA). Supersignal West Pico Plus was used as a chemiluminescent substrate (Life Technologies, Carlsbad, CA). For serum analyses, whole blood was collected from mice fed 10% and 60% fat diets and allowed to coagulate. These samples were centrifuged and the liquid fraction was collected. The isolated sera were analyzed using the mouse angiogenesis array C1 (Ray Biotech). Chemiluminescence was detected using an Azure Biosystems 600 Multimodal Imager (Dublin, CA). Densitometric analyses were performed with ImageJ 13.0.6 software.

Enzyme-Linked Immunosorbent Assays

Cells were seeded in 3cm dishes with or without dox (500ng/mL) for 3 days in full growth media. The supernatant was collected and subjected to centrifugation at 1500rpm for 10 minutes at 4°C. The levels of FGF2 secreted in the cell culture supernatant were measured using the Invitrogen™ FGF2 (bFGF) Mouse ELISA Kit (Cat# EMFGF2) according to the manufacturer's instructions. Similar approaches were used to analyze serum for mice fed 10% and 60% fat diets.

Immunohistochemistry Analyses

Primary tumors and lung sections were fixed for 24 hours in 10% neutral-buffered formalin, dehydrated in 70% ethanol, and embedded in paraffin. 5 mM sections were deparaffinized and hydrated through graded alcohol solutions and water. Citrate buffer (pH 6.0) was used for antigen retrieval and samples were blocked in hydrogen peroxide for 10 min and blocking buffer (1% BSA and 5% goat serum) for 10 minutes and rinsed with TBS-Tween (TBS-T) buffer (pH. 7.6). These sections were next incubated with Mouse Anti-Ki67 antibody (550609, BD Biosciences) at 4°C overnight. Next day, sections were rinsed with TBS-T solution (pH. 7.6) and incubated with biotinylated secondary anti-mouse antibody (Biolegend Inc., #405303) for 1 hour. Samples were incubated with ABC (VectastainÒ, Vector Laboratories #PK-6100) for 30 minutes, DAB (Vector Laboratories #SK-4100) for 5 minutes, counterstained with hematoxylin, hydrated, and mounted. H&E staining was performed by AML Laboratories (ST. Augustine, FL). Samples were visualized by using

a light microscope (Nikon Eclipse TS100, Germany) at 20x magnification and staining quantification was performed with ImageJ 13.0.6 software.

3D Growth assay

Cultrex™ Reduced Growth Factor Basement Membrane Extract, Type 2, PathClear (R&D Systems, Minneapolis, MN) was thawed at 4°C overnight and diluted (1:5) in cold serum-free medium on ice. This mixture (50 ml) was pipetted onto a 96-well plate and incubated at 37°C for 30 minutes. After polymerization, cells (2×10^3) were mixed with 10% of the Cultrex™ suspension and seeded on coated surfaces. Where indicated cells were incubated with exogenous FGF ligands (Gold Bio) (20ng/ml) or the FGFR kinase inhibitor pemigatinib. Cellular outgrowth was monitored longitudinally by bioluminescent quantification. The media was changed every third day.

3D Spheroid assay

NMuMG-GFP and FGFR1 overexpressing cells (2×10^3) were plated in 96-well, ultra-low attachment and round bottom plates (Corning) in full growth media and cultured for five days. Afterwards, the spheroids were transferred with 50µl residual media to 96-well flat clear bottom white wall plates with a bed of 50µl growth factor reduced basement membrane hydrogel and 150µl fresh media containing 5% basement membrane hydrogel with or without FGF2 (20ng/ml). Media was replenished after every 3 days. Brightfield images of spheroids were taken 9 days post FGF2 treatment using EVOS fluorescence microscope.

mRNA Analyses

For detection of FGF2 overexpression, cells (2×10^5) were seeded in triplicate 6-well plates. After 48 hours, cells were harvested and RNA was isolated (Omega Biosciences Inc. #R6812–02) and converted to cDNA conversion (Thermo Scientific, Verso cDNA Synthesis Kit #AB-1453/B). qRT-PCR analyses were completed with Maxima SYBR Green/ROX qPCR Mastermix (Thermo Scientific #K0222) by using a Biorad CFX Connect Real Time System (Biorad Laboratories, Inc.). The primer sequences (FGFR1_Fwd: 5'GCG ACC CAC ACG TCA AAC TA3', FGFR1_Rev: 5'CCG TCC ATC TTC CTT CAT AGC 3', FGF2_Fwd: 5'TTC TGG GCT GTG CTG GTC AC3', FGF2_Rev: 5'GCG AAC CTT GTA GCC TCC AA3') were obtained from the Integrated DNA Technology web site (Coralville, IA). *Gapdh* was used for normalization of gene expression levels. The relative difference in gene expression level was calculated using the δδ cycle threshold method.

Differential expression of FGFR mRNA transcripts between D2.OR and D2.A1 cells was analyzed using data accessible at NCBI GEO database (25), accession GSE172882. Graphpad prism software was used to compare the reads in transcripts per million (TPM) between the two cell lines both in 2D and 3D culture conditions.

Construction of Dox-inducible FGF2 constructs:

Human bFGF2 sequence was amplified from template plasmid (Addgene plasmid # 25812) using the following primer sequences: Fwd- CCCTCGTAAAGAATTCATGTCGAGCACCATGAAATGCAGCTGG; Rev-GATCCGCCGGCACCGGTTCAGCTCTTAGCAGACATTGGAAG. The PCR product was

purified using NucleoSpin Gel and PCR Clean-up and cloned into the TetOne-inducible expression vector pLVX-TetOne-Puro using In-Fusion HD cloning kit. Lentiviral particles were prepared using pTET-One-FGF2 plasmid, packaging vector PAX2, and envelop vector pVSVG via PEI-mediated transfection into HEK293T cells. The resultant lentiviral particles were transduced into D2OR cells using polybrene and selected using puromycin.

Statistical Analyses

All statistical analyses and graphical visualizations were completed by using Graphpad Prism9 software (GraphPad Software Inc., La Jolla, CA, www.graphpad.com). All *in vitro* experiment conditions were repeated with three independent biological repeats and at least six technical replicates, and *in vivo* experiments were repeated with at least with 3 mice/group.

Data Availability Statement

The data utilzed in this study are publicly available in Gene Expression Omnibus (GEO) at GSE172882. All other data generated in this study are available within the article and its supplementary data files.

Results:

Obesity promotes primary tumor growth and pulmonary metastasis in C57BL/6 mice

To investigate the effect of DIO on tumor progression, we separated C57BL/6 mice into two groups fed either a 10% control diet or a 60% high-fat diet (HFD). Upon observing a significant difference in body weight between 10% and 60% fat diet-fed groups, we injected syngeneic E0771 mammary tumor cells into the lateral tail vein, and pulmonary tumor formation was monitored by bioluminescent imaging (Fig. 1A–B). The group fed the HFD developed more pulmonary nodules compared to the group fed 10% fat diet as determined by significant increases in lung weight and nodule counts (Fig. 1C–E). In addition to a tail vein injection method, we also investigated the impact of DIO on primary tumor growth and the formation of spontaneous metastasis. Again, using preconditioned C57BL/6 mice, we orthotopically engrafted E0771 cells onto the 4^{th} mammary fat pad. Primary tumors were surgically removed after they reached $500mm^3$ (Fig. 1F–G). We observed that DIO resulted in mammary tumors reaching the $500mm^3$ cut-off faster (Fig. 1H–I). Spontaneous metastasis of E0771 primary tumors is not typically observed in lean animals fed standard chow. However, following primary tumor resection, several of the DIO mice went on to form large pulmonary metastases (Fig. 1H–L).

Ovariectomy and thermoneutral housing allows diet-induced obesity in Balb/c mice

To further investigate the role of DIO on metastasis we sought to evaluate additional syngeneic tumor models. However, this required the use of Balb/c mice, a strain known to be resistant to DIO (17,26–28). To expand experimental conditions recently utilized for DIO in Rag1 knockout mice. We first compared the impact of environmental temperature on DIO (8,29–31). Balb/c mice housed at thermoneutral temperature gained significantly more weight in response to a HFD compared to the mice housed at standard temperature (Fig. 2A). No differences in food intake were observed between mice housed

at thermoneutral temperature (~80°F) compared to mice housed at standard temperature (~72°F) (Fig. 2B). To better recapitulate postmenopausal conditions, we next compared DIO profiles of ovariectomized and non-ovariectomized Balb/c mice housed under thermoneutral temperatures. The addition of ovariectomy to thermoneutral housing resulted in a significant increase in weight gain in Balb/c after 15 weeks on HFD (Fig. 2C). As above, no difference was observed in food intake between these groups (Fig. 2D). To determine the functional significance of this Balb/c model of DIO we first utilized the aggressive 4T1 model of metastasis. Using the DIO protocol described above, Balb/c mice were preconditioned with 10% and 60% fat diet, resulting in a significant increase in body weight (Fig. 2E). At this point 4T1 cells were engrafted onto the 4th mammary fat pad of these Balb/c mice. Primary tumors grew at a similar rate as determined by caliper measurements and tumors were removed 25 days after injection (Fig. 2F). However, following resection, we did observe a significant increase in primary tumor weight in the 60% fat diet group (Fig. 2G–H). This discrepancy is likely due to caliper measurements of tumor volume in obese mice being less accurate than in lean mice due to adipose tissue impeding access to the tumor's full extent. Consistent with previous studies from our group and others using Balb/c mice under standard housing conditions, the 4T1 model remained aggressive in lean animals under thermoneutral housing conditions, resulting in numerous pulmonary metastases (32–34) (Fig. 2I–J). We were unable to quantify any further increase in the number of metastases in the DIO group, but we did quantify an increase in the total lung weight, suggestive of enhanced metastatic growth in the DIO animals (Fig. 2I–J).We note that while the 4T1 model did not show a dramatic increase in breast cancer progression due to obesity, there was still a consistent pattern of increased primary tumor weight and metastatic weight. These effects, although more subtle, align with the trends observed in the non-metastatic E0771 model, where the influence of obesity on tumor growth was more evident.

Diet-induced obesity prevents pulmonary dormancy

Given the metastatic nature of the 4T1 model, our ability to investigate the sufficiency of DIO on facilitating specific steps of metastasis was limited. Therefore, we next utilized the D2.OR model of pulmonary dormancy to evaluate the impact of DIO on inducing outgrowth of disseminated tumor cells (35,36). The D2.OR cell line, used to study breast cancer dormancy, displays a highly proliferative phenotype when cultured on standard tissue culture plastic. However, these cells enter into a state of dormancy using either *in vitro* 3D culture systems or *in vivo* systems (18). For instance, following tail vein injection D2.OR cells remain undetectable within the lungs for long periods, but these cells can re-activate, leading to macroscopic pulmonary tumor formation. Therefore, this model is crucial for understanding cancer dormancy and the triggers of dormant cell reactivation and metastatic tumor recurrence. Following our endocrine and thermoneutral housing approach from above Balb/c mice were separated into two groups and fed 10% or 60% fat diet until a significant difference in body weight was achieved (Fig 3A–B). In this instance, we also verified gain in fat mass using MRI (Fig. 3C). D2.OR cells were delivered to the lungs via sequential injections into the lateral tail vein and pulmonary tumor formation was tracked by bioluminescence (Fig. 3B and D). The bioluminescence signal in the lungs of the control diet group remained at or near the detectable limit demonstrating maintenance of pulmonary tumor dormancy. However, mice fed a HFD developed macroscopic pulmonary

lesions following the second injection of the D2.OR cells (Fig. 3D–E). In addition to bioluminescence (BLI) readings, nodule counts and lung weights in the DIO group were also significantly higher compared to control diet group (Fig. 3F–H). Immunohistochemical analyses indicated that there was a significantly higher frequency of Ki67-positive tumor cells in obese mice compared to the dormant lesions in lean animals (Fig. 3I–K). These results suggested that DIO can increase the progression of D2.OR allowing for the formation of macroscopic pulmonary lesions in Balb/c mice following intravenous delivery.

Diet-induced obesity increases serum levels of FGF2 in Balb/c mice

We next sought to investigate the molecular mechanisms underlying obesity-associated outgrowth of D2.OR pulmonary lesions. Utilizing a cytokine array, we evaluated differences between growth factor profiles in the serum of mice fed control and HFDs. Several growth factors and cytokines such as FGF2 and leptin were potentially increased in DIO Balb/c mice (Fig. 4A–B). To functionally assess which cytokines and growth factors can contribute to obesity-induced outgrowth of the D2.OR cells we prepared 3D cultures with D2.OR cells treated with each of the factors were found to be potentially increased in the serum of obese mice. Of the six factors tested at a fixed concentration of 20 ng/ml only FGF2 was capable of inducing outgrowth of the D2.OR cells under 3D culture conditions (Fig. 4C-upper panel, 4D). Therefore, we used an FGF2-specific ELISA to confirm increased FGF2 in the serum from DIO animals compared to their lean counterparts (Fig. 4E). To verify that FGF2 was signaling through FGF receptors (FGFR), we treated the D2.OR cultures with pemigatinib, an FDA-approved FGFR-targeted kinase inhibitor. Indeed, FGF2 stimulation of D2.OR cells caused downstream phosphorylation of ERK1/2 and this event was prevented through pretreatment with pemigatinib (Supplementary Fig.1A). Consistent with these signaling data, the use of pemigatinib prevented FGF2-induced outgrowth of D2.OR cells (Fig. 4C-lower panel, Fig. 4D). We also surveyed several other FGF ligands and found that in addition to FGF2, FGF1 and FGF9 were also capable of inducing outgrowth of the D2.OR cells under 3D culture conditions (Fig. 4F). Taken together, these data clearly demonstrate that FGF2 is increased in the serum of obese animals and can break the dormant phenotype of the D2.OR cells.

FGFR1 is required for obesity-induced outgrowth

Given the ability of FGF2 to break the dormant phenotype of the D2.OR cells, we next sought to investigate expression profiles of specific FGFRs in dormant D2.OR cells and their isogenic and metastatic counterparts, the D2.A1 cells. Analysis of GSE172882 clearly demonstrated that FGFR1 is the most abundant transcript in both D2.A1 and D2.OR cells compared FGFRs 2–4. This result was irrespective of culture under proliferative two-dimensional conditions or dormancy-inducing 3D culture conditions (Fig. 5A–5B) (25,37,38). To investigate the specific effect of FGFR1 in D2.OR dormancy, we depleted FGFR1 using two independent shRNAs. We then introduced these modified cells into Balb/c mice adhering to a high-fat diet, following the Diet-Induced Obesity (DIO) protocol established earlier in our study (Fig. 5C–D). This approach demonstrated that FGFR1 is necessary for FGF2-stimulated outgrowth of the D2.OR cells (Supplementary Fig.1B–C). Furthermore, in contrast, to control D2.OR cells, when FGFR1-depleted D2.OR cells were inoculated into the tail vein of DIO Balb/c mice, they failed to form pulmonary nodules

(Fig. 5E–I). Next, we compared the ability of serum derived from control and obese mice to modulate the outgrowth of D2.OR cells under 3D culture conditions. We observed that D2.OR cells cultured in media containing murine serum derived from DIO mice grew at a significantly higher rate than cells that were grown with serum of mice fed a control diet. Importantly, this aberrant outgrowth could be prevented with pemigatinib treatment or depletion of FGFR1 (Fig. 5J–K).

Ligand stimulation is required for outgrowth of FGFR1 overexpressing cells

To further determine the sufficiency of FGFR1 and FGF2 to induce aberrant cellular outgrowth under three-dimensional growth conditions we also stably overexpressed FGFR1 in normal murine mammary gland (NMuMG) cells. Overexpression of FGFR1 alone had no impact on the growth or morphology of NMuMG spheroids (Fig. 6A–E). Exogenous FGF2 stimulation of control NMuMG cells also did not affect cellular growth or morphology (Fig. 6A–E). However, exogenous FGF2 stimulation of FGFR1 overexpressing NMuMG cells promoted overall growth and increased the number of invasive protrusions formed by these 3D spheroids (Fig. 6A–E). Next, we again grew these cells in serum derived from control and obese mice in the presence or absence of pemigatinib. This demonstrated that FGFR1 overexpressing NMuMG cells grown in serum derived from DIO mice formed larger 3D colonies compared to the cells grown in serum derived from lean mice. This event could be prevented by pemigatinib treatment (Fig. 6F–G). Taken together with Figure 5, these results demonstrate that FGFR1 overexpression alone is not sufficient to predict a dormant versus metastatic phenotype, but FGF2 signaling through FGFR1 is sufficient to overcome a dormant phenotype.

FGFR signaling can prevent pulmonary tumor dormancy.

To further investigate the relationship between FGFR1:FGF2 signaling during *in vivo* dormancy, we generated D2.OR cells stably overexpressing FGF2 (Fig. 7A). Similar to exogenous FGF2 stimulation, overexpression of FGF2 in the D2.OR cells resulted in increased outgrowth under dormancy-inducing 3D culture conditions, and this was prevented by pemigatinib treatment (Fig. 7B–C). To verify the outgrow effect of FGF2 could be achieved in a paracrine fashion we constructed a non-luciferase expressing D2.OR cells with doxycycline-inducible expression of FGF2 (Supplementary Fig.2A). These cells were cocultured with our firefly luciferase expressing D2.OR cells under 3D culture conditions and outgrowth was tracked by bioluminescence. Indeed, upon induction of FGF2, we could observe the outgrowth of the luminescent responder cells (Supplementary Fig.2B–C). Therefore, we injected control and FGF2 overexpressing cells into the lateral tail vein of Balb/c mice and we longitudinally tracked pulmonary outgrowth by BLI (Fig. 7D–E). In contrast to the dormant phenotype of the control D2.OR cells, FGF2 overexpressing cells developed advanced pulmonary lesions as measured by bioluminescence and total lung weight (Fig. 7F–G). Consistent with macroscopic lesion formation, we observed that the frequency of Ki67-positive cells was significantly higher in FGF2 overexpressing lesions (Fig. 7H). Together with our findings from above, these results clearly demonstrate that both autocrine and paracrine FGF2 can prevent the onset of pulmonary dormancy in the D2.OR model.

Discussion:

Obesity is a significant risk factor for breast cancer recurrence and metastatic progression, especially for postmenopausal women. Although long-term survival is generally favorable, almost 30% of breast tumors eventually relapse and metastasize to distant organs after being treated with multiple therapeutic regimens (39,40). Metastatic disease causes 90% of all cancer deaths, and obesity is a contributing factor to metastasis (41). Many cohort studies have shown that postmenopausal women who are obese have a 20–40% higher risk of developing breast cancer compared to normal-weight women and weight loss intervention reduces recurrence among breast cancer patients. (42–45). However, the molecular mechanisms behind this association have not been fully elucidated.

The mechanistic understanding of how DIO drives metastatic breast progression has been limited by the lack of model systems capable of recapitulating clinical observations. Indeed, feeding of a HFD typically only results in DIO in BL6 mice, limiting tractable syngeneic tumor transfer studies to E0771 cells in the primary tumor setting (46). Consistent with prior reports, we were able to demonstrate that primary tumor growth of the E0771 cells was increased upon DIO (46–48). We extended this model through the use of tail vein inoculation and a surgical intervention approach to remove the primary tumor and continue to monitor for the development of experimental and spontaneous metastases. Indeed, systemic metastases were not observed following orthotopic engraftment of the E0771 cells in lean mice, but DIO was sufficient to induce pulmonary metastases following primary tumor removal.

To investigate additional models, we capitalized on recent studies demonstrating that ovariectomy combined with thermoneutral housing is capable of allowing for DIO in Rag1 null mice (8,29,49). Use of this approach was similarly capable of inducing DIO in the Balb/c strain, opening opportunities to evaluate additional syngeneic models of breast cancer of known metastatic potential. Here, we clearly demonstrate that DIO can advance the pulmonary dormancy phenotype of the D2.OR model to form macroscopic pulmonary lesions following tail vein inoculation. The mechanistic underpinnings of how ovariectomy and thermoneutral housing contribute to DIO remain to be established. However, this protocol of DIO will facilitate future work evaluating the impact of obesity on additional syngeneic and genetically engineered tumor models.

Through combined use of a cytokine array and 3D culture, our findings clearly point to the importance of FGFR1 signaling driving obesity-induced outgrowth of the D2.OR model. FGFR1 is amplified in up to 20% of metastatic breast cancers, however initial attempts to use this genomic event as a biomarker to apply FGFR inhibitors have not been successful (50–52). Our studies here indicate that overexpression of WT FGFR1 alone is not an efficient biomarker for application of FGFR kinase inhibitors and that high-level expression of FGFR1 is not sufficient to drive aberrant cell growth. For instance, our findings in figure 5 demonstrate that the dormant D2.OR cells actually express higher levels of FGFR1 as compared to their isogenic and metastatic D2.A1 counterpart. Additionally, ectopic overexpression of FGFR1 was not sufficient to transform normal mammary epithelial cells. These findings suggest that aberrant sources of FGFR ligands that result through

macroenvironmental changes, such as obesity, could be utilized in combination with FGFR amplification to guide clinical application of FGFR-targeted therapies in metastatic breast cancer. Along these lines, case reports of patients bearing amplification for the FGF 3/4/19 locus having complete responses to FGFR inhibition do exist (53). However, FGF 3/4/19 are not the most robust ligands for the FGFR1-iiic splice variant that we and others have demonstrated dominates metastatic tumors that have undergone EMT (54). Consistent with previous findings in other strains, our data herein demonstrate that serum levels of FGF2 increase in Balb/c mice following DIO. The source of this ligand in obese animals remains to be established. Clearly, adipose tissue is capable of producing FGF1 and FGF2. (9,46,55–58). However, FGF2 is not typically thought of as endocrine FGF as it binds tightly to heparin sulfate proteoglycans, limiting its ability to diffuse beyond its source of production (59,60). Again, consistent with our previous studies demonstrating the upregulation of autocrine FGF2 expression during EMT, our data herein demonstrate that either autocrine or paracrine FGF2 is capable of driving the outgrowth of the D2.OR cells in a pemigatinib dependent manner. Taken together, these findings are consistent with the ability of dormant D2.OR lesions to preferentially bind and respond to free FGF2 in the serum of DIO animals. However, in addition to direct effects on tumor cells, previous studies have demonstrated that increased levels of FGF2 are associated with an angiogenic switch during tumor initiation (61). While not explored here, our findings do not rule out additional impacts of FGF2 on vascularization and pulmonary tumor outgrowth under obese conditions. In contrast to these tumor initiation phenotypes, we and others have also demonstrated FGF signaling can perpetuate a mesenchymal cell state through stabilization of the transcription factor Twist. These highly mesenchymal cells can persist in the face of drug treatment but are not capable of undergoing metastatic outgrowth. What determines the overall proliferative versus mesenchymal promoting outcomes of FGF signaling in heterogeneous tumors of varying epithelial versus mesenchymal character and FGFR1 expression status remains an active area of investigation in our lab.

Finally, our findings point to the potential of pemigatinib or other FGFR-targeted therapeutics for the treatment of obesity-associated metastasis. However, the prophylactic implications of this work, following primary tumor intervention, remain difficult to foresee. Toxicities associated with pan FGFR inhibition will likely preclude the use of current FGFR inhibitors as prophylactic agents for metastatic prevention. Therefore, future studies are needed to develop strategies capable of reducing systemic FGF levels following primary tumor intervention to prolong states of remission in FGFR1-amplified breast cancer.

Overall, our study developed and utilized a novel model of DIO to illustrate the importance of a growth factor-induced mechanism of pulmonary metastatic outgrowth. Our results further illustrate a functional example of how genetic abnormalities, such as copy number alterations, should be considered in the context of patient body type and lifestyle traits when determining therapeutic interventions.

Supplementary Material

Refer to Web version on PubMed Central for supplementary material.

Acknowledgements:

E0771 cells were generous gifts from Dr. Erik Nelson (University of Illinois at Urbana-Champaign, USA). This research was supported with NCI RO1 grants (R01CA232589 and R01CA271597) and The Catherine Peachy Foundation and the Women's Global Health Institute (WGHI). We also acknowledge the expertise of the personnel within the Purdue Center for Cancer Research Biological Evaluation Core (P30CA023168). Data supporting this study are included within the article and/or supporting materials.

References:

1. Howlader N, Noone AM, Krapcho M, Miller D, Brest A, Yu M, Ruhl J, Tatalovich Z, Mariotto A, Lewis DR, SEER Cancer Statistics Review, 1975–2017, National Cancer Institute. Bethesda, MD, https://seer.cancer.gov/csr/1975_2017/, based on November 2019 SEER data submission, posted to the SEER web site, April 2020.
2. Brewster AM, Hortobagyi GN, Broglio KR, Kau SW, Santa-Maria CA, Arun B, et al. Residual Risk of Breast Cancer Recurrence 5 Years After Adjuvant Therapy. JNCI J Natl Cancer Inst. 2008 Aug 20;100(16):1179–83. [PubMed: 18695137]
3. Ewertz M, Jensen M, Gunnarsdóttir KÁ, Højris I, Jakobsen EH, Nielsen D, Stenbygaard LE, Tange UB & Cold S (2011). Journal of Clinical Oncology, 29 (1), 25–31. doi: 10.1200/JCO.2010.29.7614. [PubMed: 21115856]
4. Chan DSM, Vieira AR, Aune D, Bandera EV, Greenwood DC, McTiernan A, et al. Body mass index and survival in women with breast cancer—systematic literature review and meta-analysis of 82 follow-up studies. Ann Oncol. 2014 Oct;25(10):1901–14. [PubMed: 24769692]
5. Nies VJM, Sancar G, Liu W, van Zutphen T, Struik D, Yu RT, et al. Fibroblast Growth Factor Signaling in Metabolic Regulation. Front Endocrinol [Internet]. 2016 Jan 19 [cited 2021 Dec 17];6. Available from: http://journal.frontiersin.org/Article/10.3389/fendo.2015.00193/abstract
6. Jiao H, Arner P, Dickson SL, Vidal H, Mejhert N, Henegar C, et al. Genetic Association and Gene Expression Analysis Identify *FGFR1* as a New Susceptibility Gene for Human Obesity. J Clin Endocrinol Metab. 2011 Jun;96(6):E962–6. [PubMed: 21430024]
7. The relationship between leptin, leptin receptor, and FGFR1 in primary human breast tumors. Shoemaker Wyatt, Paithankar Shreya, Benham Vanessa, Chen Bin, and Bernard Jamie Journal of Clinical Oncology 2020 38:15_suppl, e13578–e13578.
8. Wellberg EA, Kabos P, Gillen AE, Jacobsen BM, Brechbuhl HM, Johnson SJ, et al. FGFR1 underlies obesity-associated progression of estrogen receptor–positive breast cancer after estrogen deprivation. JCI Insight. 2018 Jul 26;3(14):e120594. [PubMed: 30046001]
9. Chakraborty D, Benham V, Bullard B, Kearney T, Hsia HC, Gibbon D, et al. Fibroblast growth factor receptor is a mechanistic link between visceral adiposity and cancer. Oncogene. 2017 Nov;36(48):6668–79. [PubMed: 28783178]
10. Mejhert N, Galitzky J, Pettersson AT, Bambace C, Blomqvist L, Bouloumié A, et al. Mapping of the Fibroblast Growth Factors in Human White Adipose Tissue. J Clin Endocrinol Metab. 2010 May 1;95(5):2451–7. [PubMed: 20228166]
11. Li H, Zhang X, Huang C, Liu H, Zhang Q, Sun Q, et al. FGF2 disruption enhances thermogenesis in brown and beige fat to protect against adiposity and hepatic steatosis. Mol Metab. 2021 Dec;54:101358. [PubMed: 34710640]
12. Kakudo N, Shimotsuma A, Kusumoto K. Fibroblast growth factor-2 stimulates adipogenic differentiation of human adipose-derived stem cells. Biochem Biophys Res Commun. 2007 Jul;359(2):239–44. [PubMed: 17543283]
13. Korah R, Boots M, Wieder R. Integrin ⌙5⃣1 Promotes Survival of Growth-Arrested Breast Cancer Cells: An in Vitro Paradigm for Breast Cancer Dormancy in Bone Marrow. :9.
14. Tivari S, Lu H, Dasgupta T, De Lorenzo MS, Wieder R. Reawakening of dormant estrogen-dependent human breast cancer cells by bone marrow stroma secretory senescence. Cell Commun Signal. 2018 Dec;16(1):48. [PubMed: 30119678]
15. Benham V, Chakraborty D, Bullard B, Bernard JJ. A role for FGF2 in visceral adiposity-associated mammary epithelial transformation. Adipocyte. 2018 Mar 21;1–8.

16. Hao RH, Guo Y, Dong SS, Weng GZ, Yan H, Zhu DL, et al. Associations of Plasma FGF2 Levels and Polymorphisms in the FGF2 Gene with Obesity Phenotypes in Han Chinese Population. Sci Rep. 2016 Apr;6(1):19868. [PubMed: 26879180]
17. Ribeiro DL, Pinto ME, Maeda SY, Taboga SR, Góes RM. High fat-induced obesity associated with insulin-resistance increases FGF-2 content and causes stromal hyperplasia in rat ventral prostate. Cell Tissue Res. 2012 Aug;349(2):577–88. [PubMed: 22661309]
18. Wendt MK, Taylor MA, Schiemann BJ, Schiemann WP. Down-regulation of epithelial cadherin is required to initiate metastatic outgrowth of breast cancer. Luo K, editor. Mol Biol Cell. 2011 Jul 15;22(14):2423–35. [PubMed: 21613543]
19. Barkan D, El Touny LH, Michalowski AM, Smith JA, Chu I, Davis AS, et al. Metastatic Growth from Dormant Cells Induced by a Col-I–Enriched Fibrotic Environment. Cancer Res. 2010 Jul 15;70(14):5706–16. [PubMed: 20570886]
20. Shibue T, Brooks MW, Weinberg RA. An Integrin-Linked Machinery of Cytoskeletal Regulation that Enables Experimental Tumor Initiation and Metastatic Colonization. Cancer Cell. 2013 Oct;24(4):481–98. [PubMed: 24035453]
21. Rak J, McEachern D, Miller F. Sequential alteration of peanut agglutinin binding-glycoprotein expression during progression of murine mammary neoplasia. Br J Cancer. 1992 May;65(5):641–8. [PubMed: 1586590]
22. Brown WS, Tan L, Smith A, Gray NS, Wendt MK. Covalent Targeting of Fibroblast Growth Factor Receptor Inhibits Metastatic Breast Cancer. Mol Cancer Ther. 2016 Sep 1;15(9):2096–106. [PubMed: 27371729]
23. Chen H, Cresswell GM, Libring S, Ayers MG, Miao J, Zhang ZY, et al. Tumor Cell–Autonomous SHP2 Contributes to Immune Suppression in Metastatic Breast Cancer. Cancer Res Commun. 2022 Oct 3;2(10):1104–18. [PubMed: 36969745]
24. Akhand SS, Liu Z, Purdy SC, Abdullah A, Lin H, Cresswell GM, et al. Pharmacologic Inhibition of FGFR Modulates the Metastatic Immune Microenvironment and Promotes Response to Immune Checkpoint Blockade. Cancer Immunol Res. 2020 Dec;8(12):1542–53. [PubMed: 33093218]
25. Prunier C, Alay A, van Dijk M, Ammerlaan KL, van Gelderen S, Marvin DL, et al. Breast cancer dormancy is associated with a 4NG1 state and not senescence. Npj Breast Cancer. 2021 Dec;7(1):140. [PubMed: 34707097]
26. Rodriguez-Nunez I, Caluag T, Kirby K, Rudick CN, Dziarski R, Gupta D. Nod2 and Nod2-regulated microbiota protect BALB/c mice from diet-induced obesity and metabolic dysfunction. Sci Rep. 2017 Apr 3;7(1):548. [PubMed: 28373658]
27. Marcelin G, Liu SM, Schwartz GJ, Chua SC. Identification of a Loss-of-Function Mutation in *Ube2l6* Associated With Obesity Resistance. Diabetes. 2013 Aug 1;62(8):2784–95. [PubMed: 23557705]
28. Fearnside JF, Dumas ME, Rothwell AR, Wilder SP, Cloarec O, Toye A, et al. Phylometabonomic Patterns of Adaptation to High Fat Diet Feeding in Inbred Mice. Butler G, editor. PLoS ONE. 2008 Feb 27;3(2):e1668. [PubMed: 18301746]
29. Wellberg EA, Corleto KA, Checkley LA, Jindal S, Johnson G, Higgins JA, et al. Preventing ovariectomy-induced weight gain decreases tumor burden in rodent models of obesity and postmenopausal breast cancer. Breast Cancer Res. 2022 Dec;24(1):42. [PubMed: 35725493]
30. Maugham ML, Thomas PB, Crisp GJ, Philp LK, Shah ET, Herington AC, et al. Insights from engraftable immunodeficient mouse models of hyperinsulinaemia. Sci Rep. 2017 Mar 28;7(1):491. [PubMed: 28352127]
31. Liu X, Huh JY, Gong H, Chamberland JP, Brinkoetter MT, Hamnvik OPR, et al. Lack of mature lymphocytes results in obese but metabolically healthy mice when fed a high-fat diet. Int J Obes. 2015 Oct;39(10):1548–57.
32. Pulaski BA, Ostrand-Rosenberg S. Mouse 4T1 Breast Tumor Model. Curr Protoc Immunol [Internet]. 2000 Oct [cited 2023 Jan 20];39(1). Available from: https://onlinelibrary.wiley.com/doi/10.1002/0471142735.im2002s39
33. Schrörs B, Boegel S, Albrecht C, Bukur T, Bukur V, Holtsträter C, et al. Multi-Omics Characterization of the 4T1 Murine Mammary Gland Tumor Model. Front Oncol. 2020 Jul 23;10:1195. [PubMed: 32793490]

34. Tao K, Fang M, Alroy J, Sahagian GG. Imagable 4T1 model for the study of late stage breast cancer. BMC Cancer. 2008 Dec;8(1):228. [PubMed: 18691423]
35. Kim EJ, Choi MR, Park H, Kim M, Hong JE, Lee JY, et al. Dietary fat increases solid tumor growth and metastasis of 4T1 murine mammary carcinoma cells and mortality in obesity-resistant BALB/c mice. Breast Cancer Res. 2011 Aug;13(4):R78. [PubMed: 21834963]
36. Evangelista GCM, Salvador PA, Soares SMA, Barros LRC, Xavier FH da C, Abdo LM, et al. 4T1 Mammary Carcinoma Colonization of Metastatic Niches Is Accelerated by Obesity. Front Oncol. 2019 Sep 20;9:685. [PubMed: 31616626]
37. Barkan D, Green JE. An In Vitro System to Study Tumor Dormancy and the Switch to Metastatic Growth. J Vis Exp. 2011 Aug 11;(54):2914. [PubMed: 21860375]
38. Bushnell GG, Deshmukh AP, den Hollander P, Luo M, Soundararajan R, Jia D, et al. Breast cancer dormancy: need for clinically relevant models to address current gaps in knowledge. Npj Breast Cancer. 2021 Dec;7(1):66. [PubMed: 34050189]
39. Ecker BL, Lee JY, Sterner CJ, Solomon AC, Pant DK, Shen F, et al. Impact of obesity on breast cancer recurrence and minimal residual disease. Breast Cancer Res. 2019 Dec;21(1):41. [PubMed: 30867005]
40. Picon-Ruiz M, Morata-Tarifa C, Valle-Goffin JJ, Friedman ER, Slingerland JM. Obesity and adverse breast cancer risk and outcome: Mechanistic insights and strategies for intervention: Breast Cancer, Inflammation, and Obesity. CA Cancer J Clin. 2017 Sep;67(5):378–97. [PubMed: 28763097]
41. Massagué J, Obenauf AC. Metastatic colonization by circulating tumour cells. Nature. 2016 Jan;529(7586):298–306. [PubMed: 26791720]
42. Guo W, Key TJ, Reeves GK. Adiposity and breast cancer risk in postmenopausal women: Results from the UK Biobank prospective cohort: Adiposity and breast cancer risk. Int J Cancer. 2018 Sep 1;143(5):1037–46. [PubMed: 29569713]
43. Blair CK, Wiggins CL, Nibbe AM, Storlie CB, Prossnitz ER, Royce M, et al. Obesity and survival among a cohort of breast cancer patients is partially mediated by tumor characteristics. Npj Breast Cancer. 2019 Oct 2;5(1):33. [PubMed: 31602394]
44. Goodwin PJ, Segal RJ, Vallis M, Ligibel JA, Pond GR, Robidoux A, et al. The LISA randomized trial of a weight loss intervention in postmenopausal breast cancer. Npj Breast Cancer. 2020 Feb 21;6(1):6. [PubMed: 32133391]
45. Di Meglio A, Martin E, Crane TE, Charles C, Barbier A, Raynard B, et al. A phase III randomized trial of weight loss to reduce cancer-related fatigue among overweight and obese breast cancer patients: MEDEA Study design. Trials. 2022 Dec;23(1):193. [PubMed: 35246219]
46. Núñez-Ruiz A, Sánchez-Brena F, López-Pacheco C, Acevedo-Domínguez NA, Soldevila G. Obesity modulates the immune macroenvironment associated with breast cancer development. Hira SK, editor. PLOS ONE. 2022 Apr 26;17(4):e0266827.
47. Thangavel H, Lizardo K, Dhanyalayam D, De Assis S, Nagajyothi JF. Diets Differently Regulate Tumorigenesis in Young E0771 Syngeneic Breast Cancer Mouse Model. J Clin Med. 2023 Jan 4;12(2):413. [PubMed: 36675341]
48. Maguire OA, Ackerman SE, Szwed SK, Maganti AV, Marchildon F, Huang X, et al. Creatine-mediated crosstalk between adipocytes and cancer cells regulates obesity-driven breast cancer. Cell Metab. 2021 Mar;33(3):499–512.e6. [PubMed: 33596409]
49. Giles ED, Wellberg EA. Preclinical Models to Study Obesity and Breast Cancer in Females: Considerations, Caveats, and Tools. J Mammary Gland Biol Neoplasia. 2020 Dec;25(4):237–53. [PubMed: 33146844]
50. Krook MA, Reeser JW, Ernst G, Barker H, Wilberding M, Li G, et al. Fibroblast growth factor receptors in cancer: genetic alterations, diagnostics, therapeutic targets and mechanisms of resistance. Br J Cancer. 2021 Mar 2;124(5):880–92. [PubMed: 33268819]
51. Mouron S, Manso L, Caleiras E, Rodriguez-Peralto JL, Rueda OM, Caldas C, et al. FGFR1 amplification or overexpression and hormonal resistance in luminal breast cancer: rationale for a triple blockade of ER, CDK4/6, and FGFR1. Breast Cancer Res. 2021 Dec;23(1):21. [PubMed: 33579347]

52. Kommalapati A, Tella SH, Borad M, Javle M, Mahipal A. FGFR Inhibitors in Oncology: Insight on the Management of Toxicities in Clinical Practice. Cancers. 2021 Jun 13;13(12):2968. [PubMed: 34199304]

53. Ileana Dumbrava E, Alfattal R, Miller VA, Tsimberidou AM. Complete Response to a Fibroblast Growth Factor Receptor Inhibitor in a Patient With Head and Neck Squamous Cell Carcinoma Harboring FGF Amplifications. JCO Precis Oncol. 2018 Aug 31;2:PO.18.00100.

54. Wendt MK, Taylor MA, Schiemann BJ, Sossey-Alaoui K, Schiemann WP. Fibroblast growth factor receptor splice variants are stable markers of oncogenic transforming growth factor β1 signaling in metastatic breast cancers. Breast Cancer Res BCR. 2014;16(2):R24. [PubMed: 24618085]

55. Ma Y, Kakudo N, Morimoto N, Lai F, Taketani S, Kusumoto K. Fibroblast growth factor-2 stimulates proliferation of human adipose-derived stem cells via Src activation. Stem Cell Res Ther. 2019 Dec;10(1):350. [PubMed: 31775870]

56. Castillo-Castrejon M, Sankofi BM, Murguia SJ, Udeme A ama, Cen HH, Xia YH, et al. FGF1 supports glycolytic metabolism through the estrogen receptor in endocrine-resistant and obesity-associated breast cancer. Breast Cancer Res. 2023 Aug 22;25(1):99. [PubMed: 37608351]

57. Nies VJM, Struik D, Liu S, Liu W, Kruit JK, Downes M, et al. Autocrine FGF1 signaling promotes glucose uptake in adipocytes. Proc Natl Acad Sci. 2022 Oct 4;119(40):e2122382119.

58. Mathes S, Fahrner A, Ghoshdastider U, Rüdiger HA, Leunig M, Wolfrum C, et al. FGF-2–dependent signaling activated in aged human skeletal muscle promotes intramuscular adipogenesis. Proc Natl Acad Sci. 2021 Sep 14;118(37):e2021013118.

59. Forsten-Williams K, Chua CC, Nugent MA. The kinetics of FGF-2 binding to heparan sulfate proteoglycans and MAP kinase signaling. J Theor Biol. 2005 Apr;233(4):483–99. [PubMed: 15748910]

60. Fernig DG, Chen HL, Rahmoune H, Descamps S, Boilly B, Hondermarck H. Differential regulation of FGF-1 and −2 mitogenic activity is related to their kinetics of binding to heparan sulfate in MDA-MB-231 human breast cancer cells. Biochem Biophys Res Commun. 2000 Jan 27;267(3):770–6. [PubMed: 10673367]

61. Roy R, Yang J, Shimura T, Merritt L, Alluin J, Man E, et al. Escape from breast tumor dormancy: The convergence of obesity and menopause. Proc Natl Acad Sci. 2022 Oct 11;119(41):e2204758119.

Implications statement:

Overall, this study developed a novel DIO model that allowed for demonstration of FGF2:FGFR1 signaling as a key molecular mechanism connecting obesity to breakage of systemic tumor dormancy and metastatic progression.

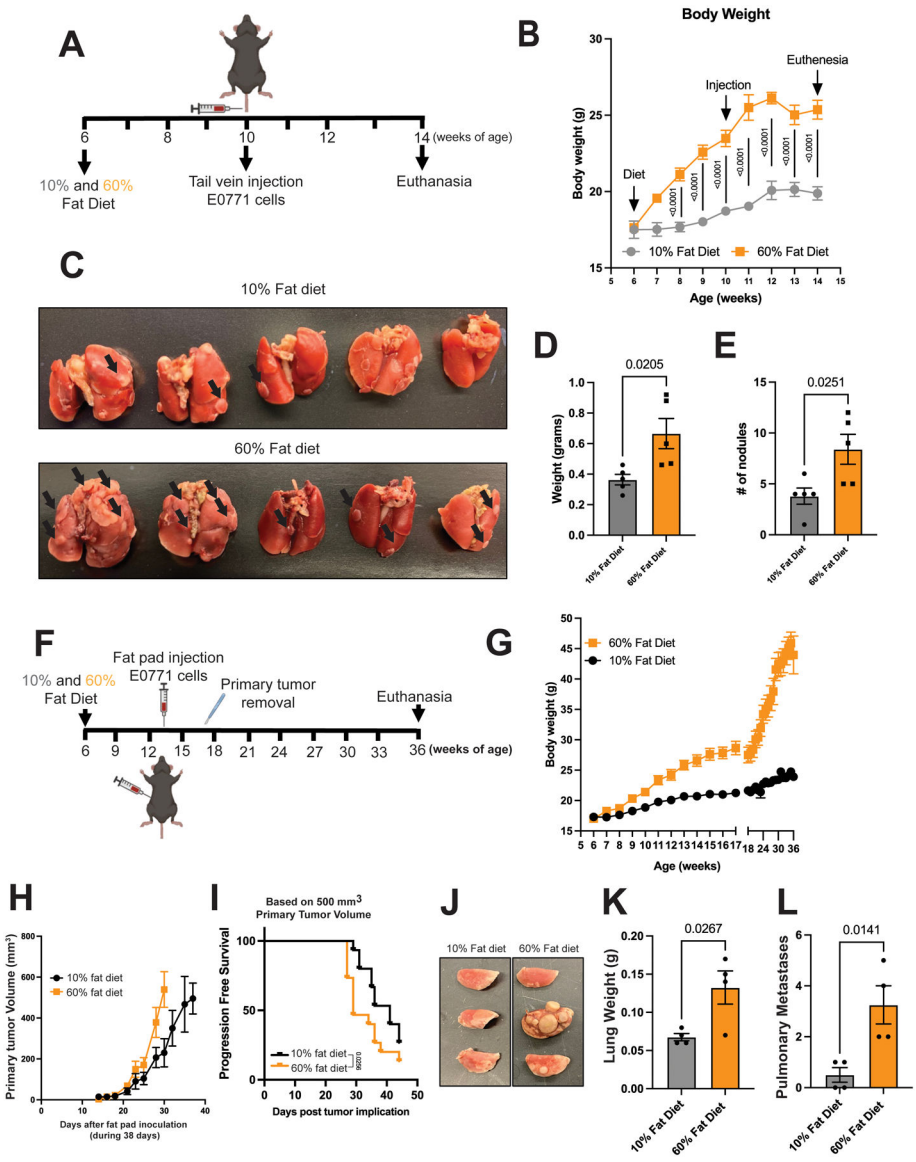

Figure 1: Obesity promotes primary tumor growth and pulmonary metastasis.

(A) Six-week-old C57BL/6 mice were fed with 10% and 60% fat diets (n=5/group). These animals were then injected via lateral tail vein with 1×10^6 luciferase expressing E0771 cells. Pulmonary tumor growth was monitored by BLI. **(B)** Body weight measurements of mice fed control and HFD were taken at the indicated time points. **(C)** Lungs from tumor-bearing mice were isolated, fixed and visualized for nodule formation (arrows). **(D)** Lung weights and **(E)** nodule counts of tumor-bearing lungs were quantified. **(F)** Six-week-old C57BL/6 mice were (n=4/group) fed 10% and 60% fat diet. Luciferase expressing E0771 cells were engrafted onto the mammary fat pad of these mice. Primary mammary tumors were removed at 500 mm^3, and formation of pulmonary metastases was monitored by BLI. **(G)** Body weight measurements were taken at the indicated time points. **(H)** Primary tumor volumes in mice receiving 10% and 60% fat diet were measured at the indicated time points. **(I)** Progression free survival of both groups based on a 500mm^3 primary tumor cut off volume.

(J-L) Upon necropsy lungs were isolated, fixed, visualized, weighed, and analyzed for number of metastases. Statistical analyses were done by using multiple t-test, unpaired t-test, and log-rank test resulting in the indicated P values.

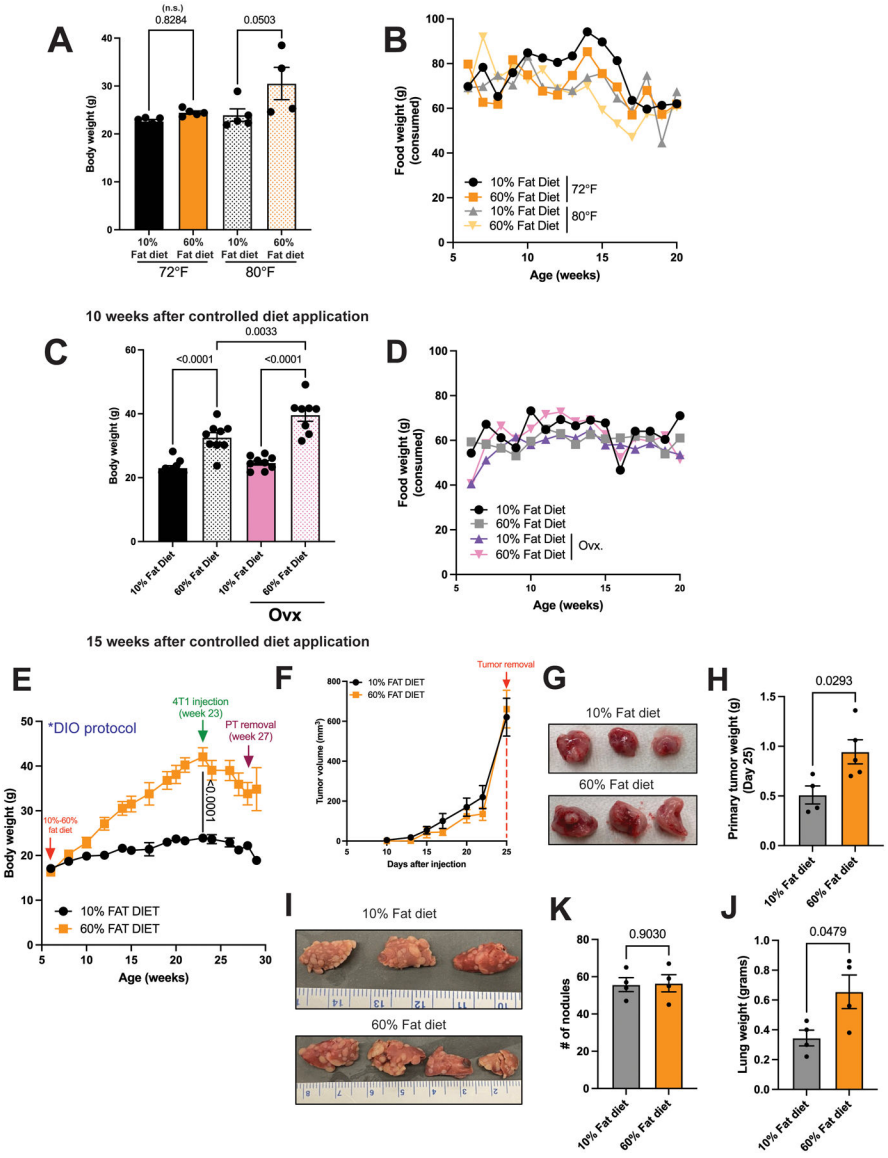

Figure 2: Ovariectomy and thermoneutral housing allows diet-induced obesity in Balb/c mice.

(A) Body weight measurements of mice housed at 72°F and 80°F were compared 10 weeks after feeding 10% and 60% fat diets (n=5/group). **(B)** Weekly food consumption by all mice was monitored during the study. **(C)** Body weight measurements of ovariectomized and non-ovariectomized Balb/c mice were measured after 15 weeks of diet intervention and thermoneutral housing. **(D)** Weekly food weight consumption by these mice was monitored during the study (n=8/group). **(E)** Six-week-old, ovariectomized, Balb/c mice housed at 80°F were fed 10% and 60% fat diet. 4T1 (5×10^4) cells were engrafted onto the mammary fat pad and primary tumors were removed at the indicated time points. **(F)** Primary tumor volumes were measured using digital calipers at the indicated time points. (**G-H)** Primary mammary tumors from mice fed with 10% and 60% fat diet were surgically removed, visualized, and weighed. **(I-J)** Three weeks after primary tumor removal, the lungs were isolated, fixed, visualized, evaluated for the number of metastases, and weighed. Statistical

analyses were done by using multiple t-test and unpaired t-test resulting in the indicated P values.

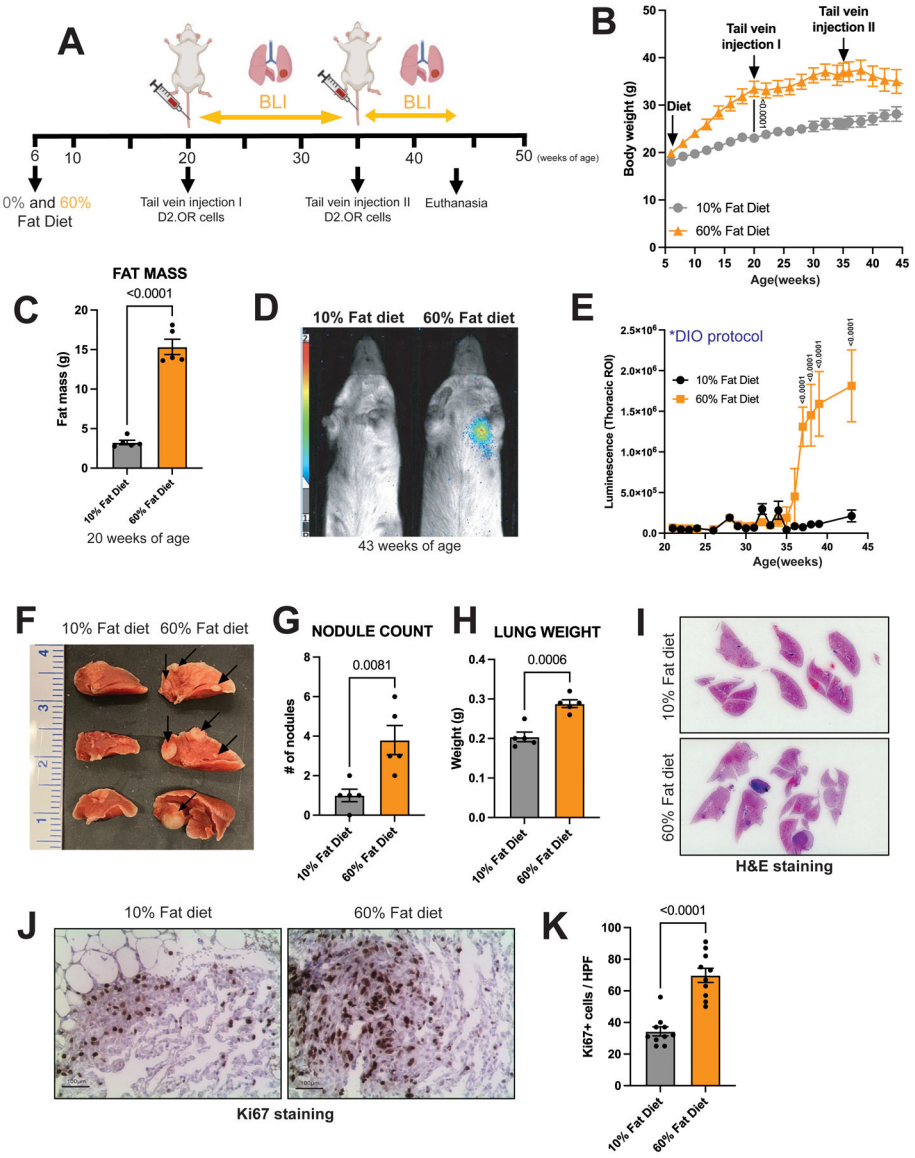

Figure 3: Diet-induced obesity prevents pulmonary dormancy.

(A) Six-week-old ovariectomized Balb/c mice housed at 80°F (n=5/group) were fed 10% or 60% fat diet. Mice were injected via the lateral tail vein with D2.OR cells (1×10^6) at indicated time points. Pulmonary tumor growth was tracked by BLI. **(B)** Body weight measurements were taken at the indicated time points. **(C)** Percent fat mass values of these mice were determined by using EchoMRI prior to tumor cell inoculation. **(D)** Representative pulmonary tumor formation visualized by BLI. **(E)** Thoracic BLI values were measured at the indicated time points. **(F-H)** Upon necropsy, lungs were isolated, fixed, visualized, analyzed for numbers of nodules, and weighed. **(I)** Representative H&E staining of histological sections from 3 mice of each group. **(J)** Representative immunohistochemical staining for Ki67 in lung sections from both groups. **(K)** Quantification of Ki67 staining frequency from at least 10 representative images from 5 separate mice per group. Data were analyzed using unpaired t-tests resulting in the indicated P values.

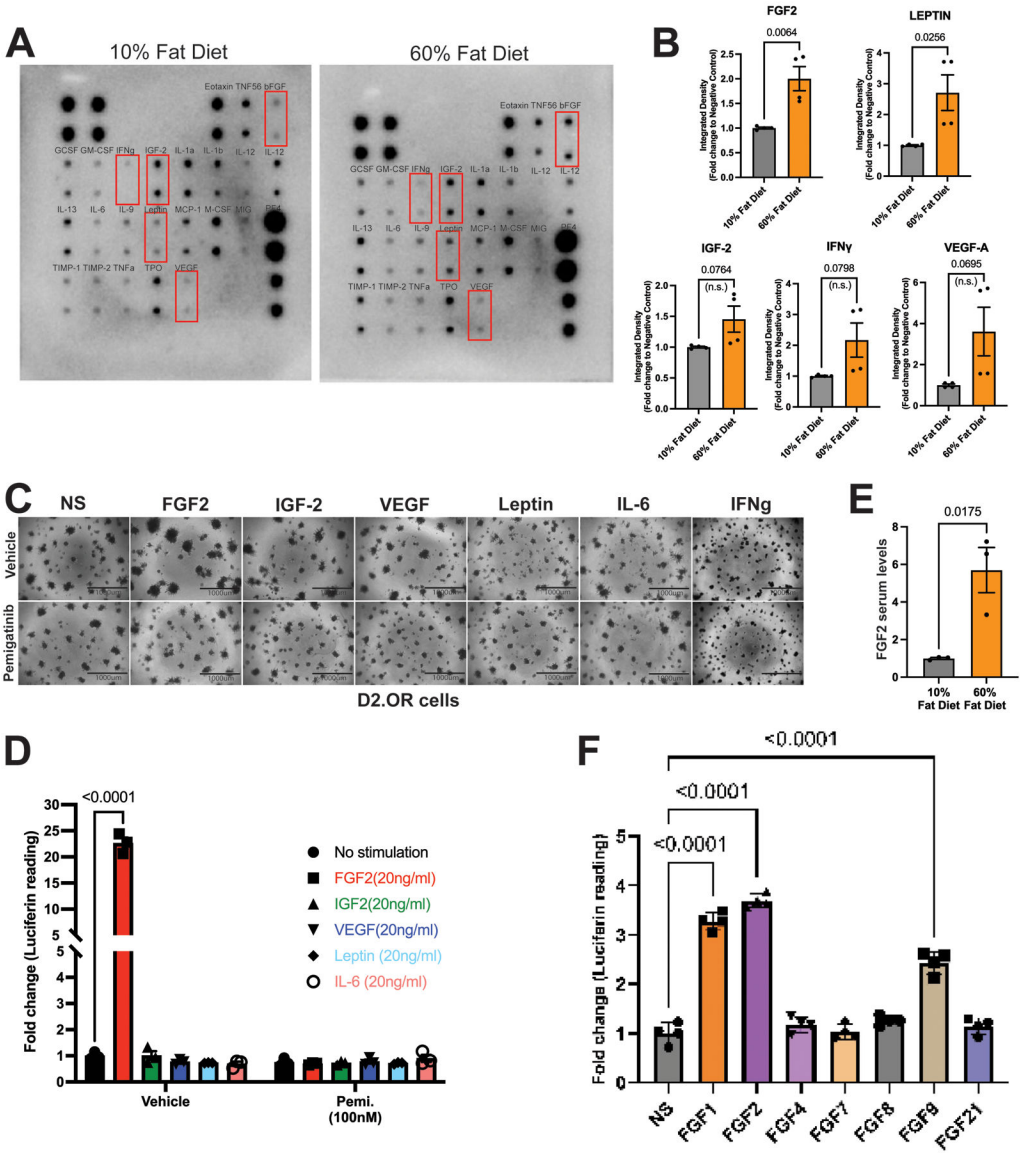

Figure 4: Diet-induced obesity increases serum levels of FGF2 in Balb/c mice.

(A) An angiogenesis cytokine array was used to compare ligand levels in serum samples taken from ovariectomized mice housed at 80°F that were fed with either 10% or 60% fat diet. **(B)** Quantification of dot blots showing differential ligand levels. **(C)** ELISA quantification of FGF2 levels in serum samples taken from mice fed 10% and 60% fat diet. Data were normalized to the 10% fat diet serum. **(D)** Images taken from 3D growth assays of D2.OR cells treated with the indicated ligands in the presence or absence of pemigatinib (100nM). **(E)** Bioluminescent quantification of 3D growth assays shown in panel D. All results were normalized according to the no stimulation (NS) group. **(F)** Bioluminescent values of the D2.OR cells were cultured for 6 days under 3D culture conditions in the presence or absence of the indicated FGF ligands (20 ng/ml). Statistical analyses were done by using unpaired t-test and one-way-ANOVA tests resulting in the indicated P values.

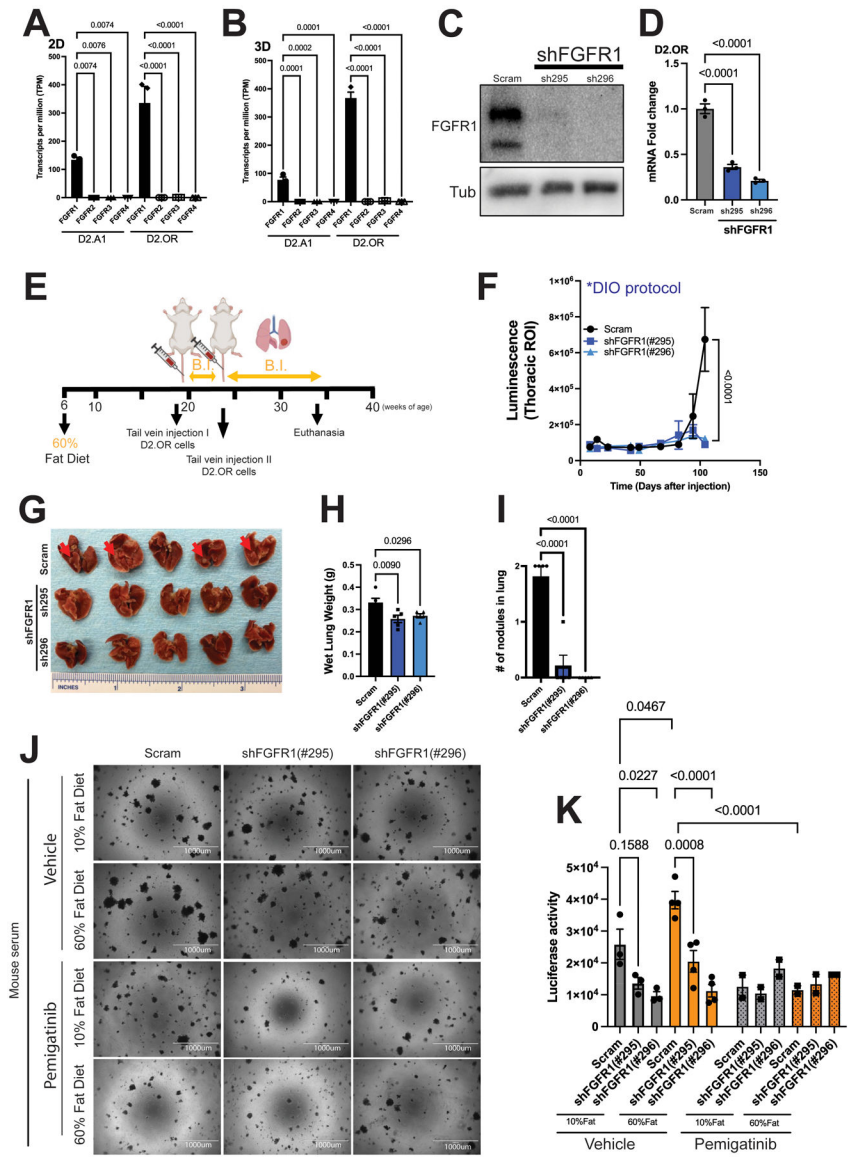

Figure 5: FGFR1 is required for obesity-induced outgrowth.

(A-B) Differential expression of FGFR1–4 mRNA transcripts between D2.OR or D2.A1 cells grown under 2D and 3D culture conditions (GSE172882). **(C)** FGFR1 immunoblot and **(D)** RT-PCR analyses of D2.OR cells expressing control (scram) and FGFR1-targeted (shFGFR1#295, shFGFR1 #296) shRNAs. β-Tubulin served as a loading control in panel C. **(E)** Six-week-old ovariectomized Balb/c mice housed at 80°F were preconditioned with 60% fat diet and were subsequently injected with control (scram) and FGFR1-depleted D2.OR cells at the indicated time points (n=5/group). **(F)** Thoracic BLI values were collected at the indicated time points after injecting cells. **(G-I)** Upon necropsy, lungs were isolated, fixed, visualized, weighed, and tumor nodules were enumerated. **(J)** Images taken from 3D growth assays of D2.OR cells in serum from ovariectomized mice housed at 80°F that were fed with 10% or 60% fat diet in the presence or absence of 100nM pemigatinib treatment for 8 days. **(K)** Bioluminescent quantification of assays described in

panel J. Statistical analyses were done by using one-way-ANOVA and two-way-ANOVA tests resulting in the indicated P values.

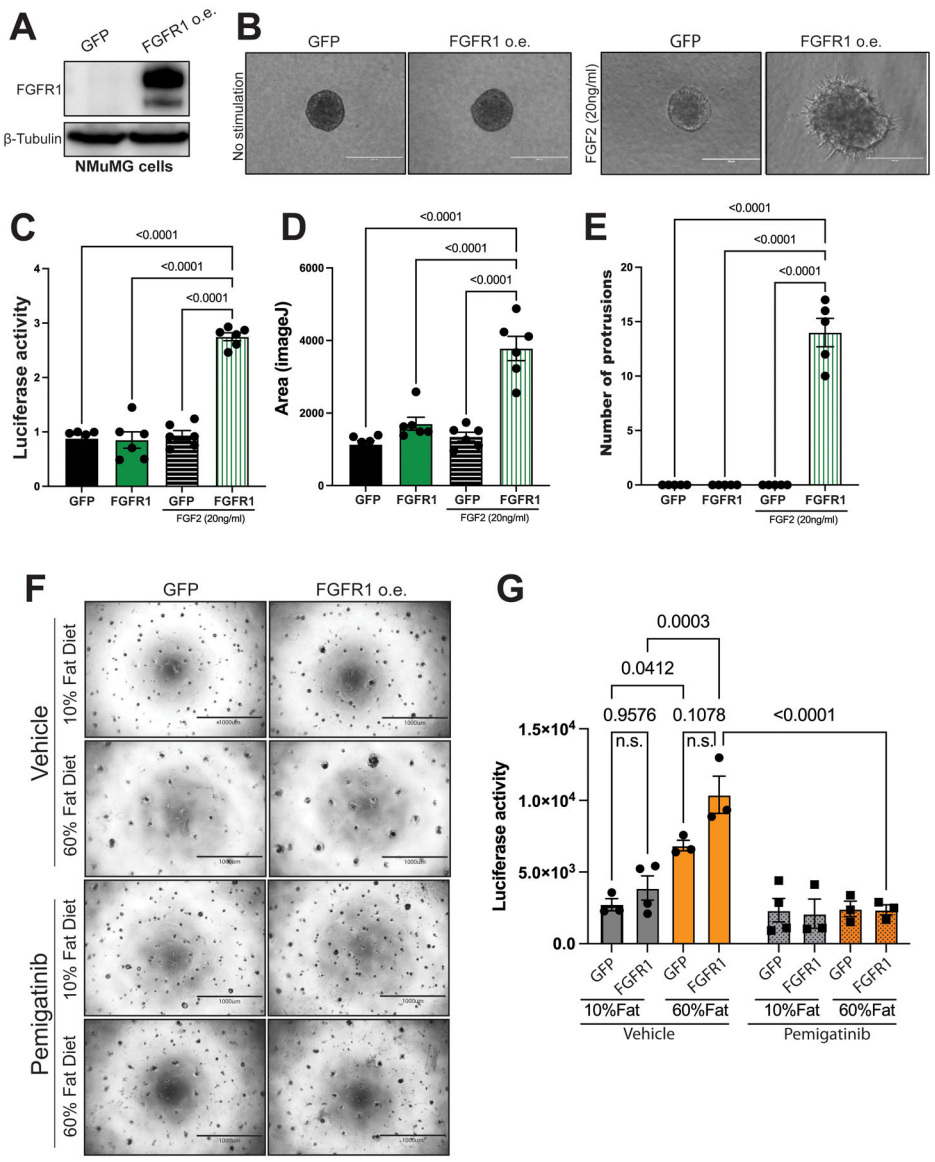

Figure 6: Ligand stimulation is required for outgrowth of FGFR1 overexpressing cells.

(A) Immunoblot analysis of FGFR1 and β-Tubulin proteins in control (GFP) NMuMG cells and those constructed to overexpress (o.e.) FGFR1**. (B)** Images of 3D spheroid assays prepared with control (GFP) and FGFR1-overexpressing NMuMG cells in the presence or absence of exogenous FGF2 (20ng/ml) stimulation for 9 days. Spheroids shown in panel B were quantified using normalized bioluminescence **(C)**, area occupied by spheroids **(D),** and number of cellular protrusions **(E). (F)** Images taken from 3D culture assays using control (GFP) and FGFR1-o.e. NMuMG cells grown in serum derived from mice fed 10% or 60% fat diet, in the presence or absence of pemigatinib treatment for 8 days. **(G)** Bioluminescent quantification of cultures described in panel F. Statistical analyses were done by using one-way-ANOVA and two-way-ANOVA tests resulting the indicated P values.

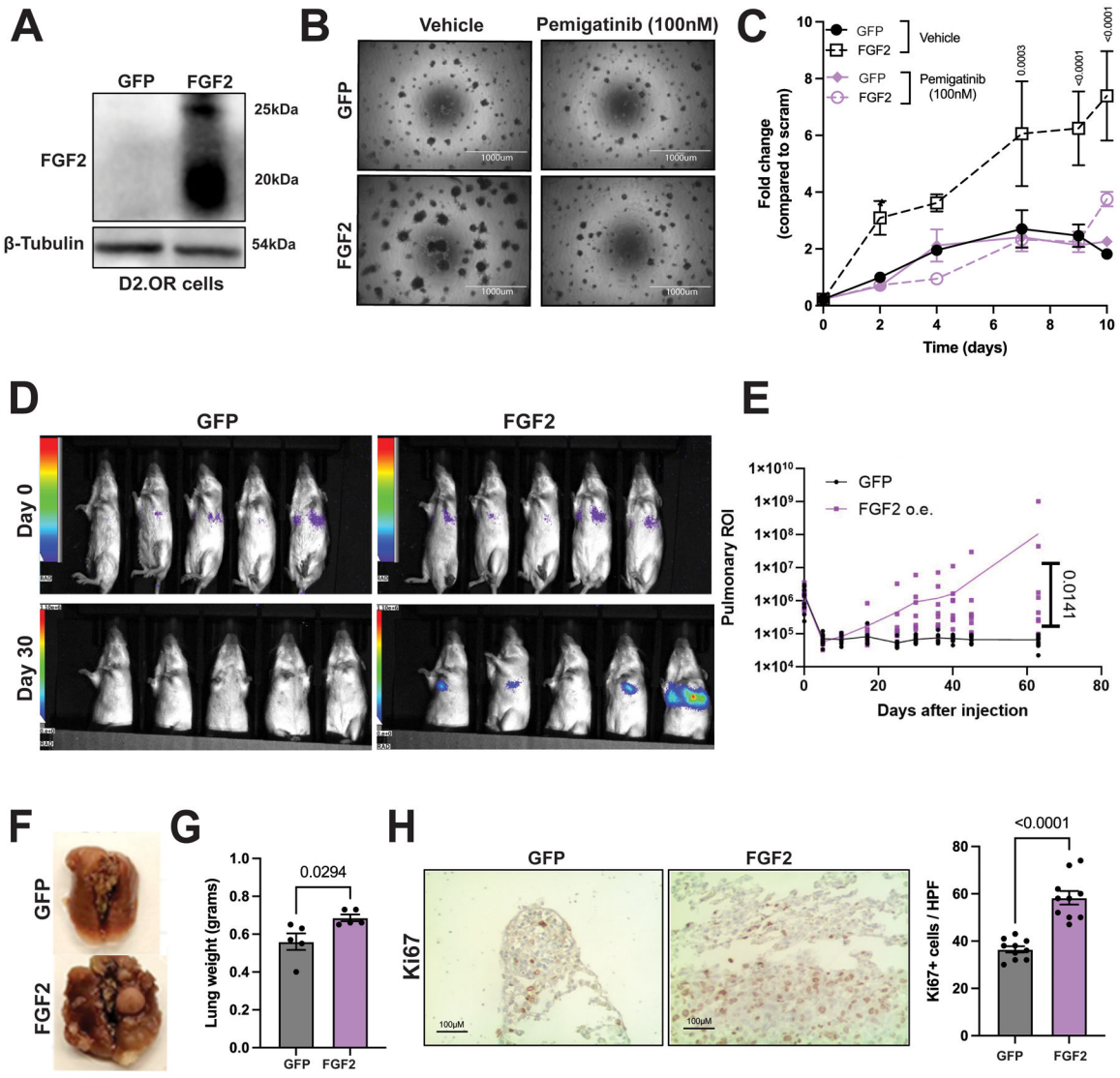

Figure 7: FGFR signaling can prevent pulmonary tumor dormancy.

(A) Immunoblot analysis for FGF2 in whole cell lysates of control (GFP) and FGF2 expressing D2.OR cells. β-Tubulin served as a loading control. **(B)** Images of 3D growth assays of control and FGF2 expressing cells. **(C)** Longitudinal bioluminescent quantification of 3D cell growth by control and FGF2 expressing D2.OR cells cultured in the presence or absence of pemigatinib. **(D)** BLI of Balb/c mice immediately (Day 0) and 30 days after (Day 30) receiving 1×10^6 control (GFP) or FGF2-expressing (FGF2) D2.OR cells via the lateral tail vein. **(E)** Pulmonary tumor growth was longitudinally quantified by BLI at the indicated time points (n=10 mice per group). **(F and G)** Upon necropsy, lungs were isolated, fixed, visualized and weighed. **(H)** Fixed lungs were sectioned and immunostained for Ki67. The frequency of Ki67 positive cells was quantified in at least 10 representative images from 5 separate mice per group. Statistical significance between groups were analyzed using unpaired t-test and one-way-ANOVA tests resulting in the indicated P-values.